



Bundle Block Adjustment of CBERS-2B HRC Imagery Combining Control Points and Lines

ANTONIO M. G. TOMMASELLI & JOSÉ MARCATO JUNIOR, Presidente Prudente, Brasil

Keywords: Orbital images, control straight lines, indirect image orientation, CBERS images, multi-feature control

Summary: The aim of this work is to present the results of the assessment of rigorous bundle block adjustment models for orbital imagery of the High-Resolution Camera (HRC) of the CBERS (China-Brazil Earth Resources Satellite). The work is focused on the experimental assessment of the combined use of ground control points (GCP) and ground control lines (GCL) in a block adjustment. The mathematical models relating object and image spaces are based on collinearity (for points) and coplanarity (for lines) conditions with polynomial modelling of the spacecraft trajectory and attitude. These models were implemented in the software TMS (triangulation with multiple sensors) with multi-feature control (GCPs and GCLs) developed in-house. Experiments on a block of four CBERS-2B HRC images were accomplished using both GCPs and GCLs. The results show that the combination of the collinearity and coplanarity models can provide better results in the bundle block adjustment process than conventional bundle adjustment with GCPs only. A systematic error in the inner geometry of HRC camera caused by the displacement of one of the three CCD sensors and the lack of proper correction when fusing the three images to generate level 1 images was also verified. Experiments to evaluate the effects of this systematic error are also presented.

Zusammenfassung: Bündelblockausgleichung von CBERS-2B HRC Bilddaten mit Passpunkten und Passlinien. Ziel dieser Arbeit ist die Präsentation der Ergebnisse einer strengen Bündelblockausgleichung für Bilder, die mit der hochauflösenden Kamera (HRC) des Satelliten CBERS (China-Brazil Earth Resources Satellite) aufgenommen wurden. Der Schwerpunkt liegt auf der experimentellen Validierung des kombinierten Einsatzes von Passpunkten (PP) und -linien (PL) in der Blockausgleichung. Die mathematischen Modelle zur Verknüpfung von Objekt- und Bildraum basieren auf Kollinearitäts- (für Punkte) bzw. Komplanaritätsbedingungen (für Linien), wobei Flugbahn und Drehwinkel des Satelliten mit Polynomen modelliert werden. Diese Modelle wurden in der Software TMS (Triangulation mit multiplen Sensoren) mit Anpassung an unterschiedliche Pass-Merkmale (PP und PL) implementiert. Experimente für einen Block aus vier CBERS-2B HRC Bildern wurden unter Verwendung sowohl von PP als auch von PL durchgeführt. Die Ergebnisse zeigen, dass die Kombination von Kollinearitäts- und Komplanaritätsmodell in der Bündelblockausgleichung bessere Ergebnisse liefern kann als das übliche Modell unter ausschließlicher Verwendung von PP. Es wurde auch ein systematischer Fehler in der inneren Geometrie der HRC-Kamera verifiziert, der durch eine Verschiebung eines der drei CCD-Sensoren und das Fehlen einer angemessenen Korrektur bei der Fusion der drei Bilder zu einem Level 1 Bild verursacht wird. Experimente zur Untersuchung der Auswirkungen dieses systematischen Fehlers werden ebenfalls präsentiert.

1 Introduction

Earth observation and analysis from space imagery became feasible in the 1970s with

Landsat program for remote sensing purposes. In 1988, Brazil and China started the CBERS (China-Brazil Earth Resources Satellite) program aiming to foster the technologi-

cal development in the field of Remote Sensing. One advantage of this program is that images acquired of South American and African territories are freely distributed. Besides the sensors CCD and WFI (Wide Field Imager), CBERS-2B carried a High-Resolution Camera (HRC), providing images with a GSD (ground sample distance) of 2.7 meters. Although the CBERS-2B satellite ceased operations on April 16, 2010, the images in archives are still of crucial importance to users in Brazil for several applications including medium-scale mapping and to compensate for the lack of other imagery.

To improve their georeferencing accuracy, orbital imaging systems are equipped with direct orientation sensors. CBERS-2B had a single-frequency GPS receiver and a star track sensor. One problem that reduced positional accuracy of CBERS-2B imagery was the lack of star sensor data, probably due to electronic failures in the area of the South Atlantic Anomaly. As a consequence, the images distributed by INPE (Brazilian National Institute for Space Research) have a positioning error larger than one kilometre in some images that were assessed. To use CBERS-2B HRC images for mapping purposes, it is necessary to indirectly estimate the orientation elements using ground control elements in the object space (points, lines and/or areas).

This camera was not originally designed to provide stereoscopic coverage, though cross-track images present an overlap with a base-to-height (B/H) ratio of approximately 0.13, considering adjacent passages. More details about CBERS-2B orbit and HRC features can be found in (INPE 2011). With this weak intersection geometry, insertion of tie points does not improve the results. It is also important to mention that CBERS-2B HRC images present small dynamic ranges (approximately 40 grey values), causing an error of approximately 1–3 pixels in the interactive measurement of the image points and lines (MARCATO JUNIOR et al. 2010).

CBERS-2B HRC has three CCDs in the focal plane that are not aligned. The central CCD is displaced by 26 mm along the flying direction, and this displacement can cause interior orientation errors, even when considering that a virtual image is generated by stitch-

ing the three partial scans. BALTSAVIAS et al. (2006) performed an investigation of the errors in DTMs generated by Ikonos Triplets and concluded that the changes in the relative displacement of the three CCDs caused height jumps in the DTM.

The orientation of pushbroom images can be performed using several techniques, mainly based on physical or empirical models (RADHADEVI et al. 1994, FRITSCH & STALLMANN 2000, DOWMAN & MICHALIS 2003, TOUTIN 2004, FRASER & HANLEY 2005, TOUTIN 2006, KIM & DOWMAN 2006, POLI 2007, WESER et al. 2008, ROTTENSTEINER et al. 2009, TONG et al. 2010, LIU et al. 2011). Physical models are generally based on bundle adjustment with adapted collinearity equations using ground control points (GCPs). Empirical models are mostly based on rational function models (RFMs), the coefficients of which are normally supplied by the image vendor.

The physical models can use either position and rotation angles as model parameters or ephemerides (position and velocity) and attitude angles (KIM & DOWMAN 2006). Independently from the used model, ground control entities are required to compute the orientation parameters or to correct the coefficients of the RFM to achieve accuracy compatible to the image spatial resolution.

For the indirect orientation of pushbroom images, the number of GCPs must be sufficient to provide redundancy to estimate the parameters by the least-squares method. Considering 12 exterior orientation parameters (EOP) (see section 2), at least 6 GCPs (with no redundancy) per image are required; however, the operational practice is to achieve at least 20 GCPs for each scene. This large number of GCPs may impact the overall costs of the projects, depending on the required accuracy and area extension. When accurate orbital information (platform position, velocity and attitude) is available, this information can be used either to provide observations/constraints in the bundle adjustment or to generate the coefficients of the RFM, reducing the number of required GCPs.

Another alternative is to use linear features as control entities. Previous works (MULAWA & MIKHAIL 1988, HABIB et al. 2002, TOMMASELLI & MEDEIROS 2010) showed the advantages of

using ground control lines (GCLs) as alternatives to GCPs, but the simultaneous adjustment with these types of ground data has not yet been assessed for CBERS-2B HRC.

Ground surveying of lineal entities is much easier and faster than surveying of GCPs for the indirect orientation of images with the spatial resolution of HRC. For example, road centre lines can be surveyed very quickly and with suitable accuracy with kinematic GPS positioning, while travelling between control point areas. Thus, the combination of both sources of ground control entities can be considered as a relevant practice to maximise the number of control entities while maintaining almost the same costs.

The aim of this work is to present the results of the assessment of rigorous bundle block adjustment models for CBERS-2B HRC imagery using points and lines as control elements. Additionally, the effects of the CCD displacements in the results of the bundle adjustment will be assessed.

2 Background – Mathematical Model

Indirect orientation of satellite images with bundle block adjustment was first carried out with SPOT across-track stereo images (TOUTIN & ROCHON 1986). Similar techniques have been used for images acquired by different satellites such as Landsat, Kompsat, QuickBird and ALOS (TOUTIN 2003, KIM & DOWMAN 2006, POLI 2007).

Pushbroom sensors generate a one-dimensional image at each instant. Orbital platforms are more stable than an airborne scanner, and thus, the EOP can be modelled with polynomials using either position and rotation angles or orbit and attitude angles as parameters (KIM & DOWMAN 2006).

In the case of pushbroom sensors, there are six unknowns for each image row. These six unknowns can be directly determined during the image acquisition using GNSS, inertial sensors, solar sensors and stellar cameras, or they can be estimated indirectly, using some source of ground control.

Several different mathematical models have been proposed for the orientation and geomet-

ric correction of pushbroom imagery. The physical models used in this work are based on the geometric properties of the acquisition process and generally use collinearity equations with some extensions.

Line-coplanarity models were also developed for the orientation of frame and pushbroom imagery (MULAWA & MIKHAIL 1988, HABIB et al. 2002, SHIN et al. 2007). These models are based on the coplanarity between the projection ray (vector from the perspective centre to the image point), the instantaneous perspective centre and the corresponding straight object line (Fig. 1).

One problem with CBERS-2B HRC images is the accuracy of their direct georeferencing, mainly caused by attitude angles errors (YU et al. 2008). YU et al. (2008) presented a calibration model to eliminate constant angular errors with sparse control. Even applying this method, errors of approximately 20 GSDs in the check points were observed.

Thus, it is necessary to correct these images with accurate position and orientation data, which can be estimated with dense control entities, such as control points or straight control lines. Although points are generally used as control elements in bundle adjustment, some advantages also motivate the use of linear features (TOMMASELLI & TOZZI 1996, HABIB & MORGAN 2003) for the following reasons:

- Image lines are easily found in man-made environments.
- The correspondence between points from image and object lines is not necessary.
- Image lines can be extracted with sub-pixel precision.

HABIB et al. (2001) also showed that the use of straight lines as constraints in the bundle adjustment of images acquired by linear array scanners provides a better estimation of the EOP when compared to those methods that use only distinct points. As a consequence of the linear scanner array geometry, lines that are straight in the object space do not appear as straight lines in the scanned images. Thus, the application of the straight-line constraints for this type of sensor is particularly important, since it increases the geometric strength of the adjustment.

In this paper, the mathematical models relating object and image spaces are based on

collinearity (for points) and coplanarity (for lines) conditions with polynomial modelling of the sensor trajectory and attitude. These models will be presented in the next sections.

2.1 Collinearity Model with Points (CMP)

The collinearity model with points (CMP) for pushbroom sensors was developed based on the collinearity condition between a point in the object space, its homologue in the image space and the instantaneous perspective centre (PC) corresponding to the image row that contains this point. (1) expresses the collinearity model for the pushbroom geometry (GUGAN & DOWMAN 1988).

$$0 = -f \frac{r_{11}(X_i - X_S) + r_{21}(Y_i - Y_S) + r_{31}(Z_i - Z_S)}{r_{13}(X_i - X_S) + r_{23}(Y_i - Y_S) + r_{33}(Z_i - Z_S)}$$

$$y_i = -f \frac{r_{12}(X_i - X_S) + r_{22}(Y_i - Y_S) + r_{32}(Z_i - Z_S)}{r_{13}(X_i - X_S) + r_{23}(Y_i - Y_S) + r_{33}(Z_i - Z_S)} \quad (1)$$

where y_i is the image coordinate in the instantaneous photogrammetric reference system of a point i in an image row j acquired in an instant t . The x coordinate is zero because the x axis of the instantaneous photogrammetric reference system is oriented in the flying direction. X_p, Y_p, Z_p are the 3D coordinates of the corresponding point in the object space; X_s, Y_s, Z_s are the instantaneous coordinates of the camera PC, corresponding to the image row j , and these values are modelled by a time dependent polynomial (3); r_{ki} are the elements of the instantaneous rotation matrix R_j from image space reference system to object space reference system corresponding to an image row j . The rotation matrix R_j is given in (2), in which s and c denotes the *sin* and *cos*, respectively.

$$R_j = \begin{bmatrix} c\kappa_j c\varphi_j & c\kappa_j s\varphi_j s\omega_j + s\kappa_j c\omega_j & -c\kappa_j s\varphi_j c\omega_j + s\kappa_j s\omega_j \\ -s\kappa_j c\varphi_j & -s\kappa_j s\varphi_j s\omega_j + c\kappa_j c\omega_j & s\kappa_j s\varphi_j c\omega_j + c\kappa_j s\omega_j \\ s\varphi_j & -c\varphi_j s\omega_j & c\varphi_j c\omega_j \end{bmatrix} \quad (2)$$

In (3), the instantaneous EOP for each image row are modelled by second-order polynomials (ORUN & NATARAJAN 1994):

$$\begin{aligned} X_S &= X_0 + a_1 t + b_1 t^2 \\ Y_S &= Y_0 + a_2 t + b_2 t^2 \\ Z_S &= Z_0 + a_3 t + b_3 t^2 \\ \kappa &= \kappa_0 + a_4 t + b_4 t^2 \\ \varphi &= \varphi_0 \\ \omega &= \omega_0 \end{aligned} \quad (3)$$

where X_0, Y_0, Z_0 are the PC coordinates and $\kappa_0, \varphi_0, \omega_0$ are the rotation angles for the first image row; a_i and b_i ($i \in [1, \dots, 4]$) are polynomial coefficients; t is a time-dependent parameter, which can be the image row number, with sub-pixel precision. The parameters a_i and b_i will absorb the scale difference between time and a float number representing the image row.

To avoid the simultaneous estimation of highly correlated pairs of parameters (e.g., φ and X_0 , ω and Y_0), the φ_0 and ω_0 angles were not considered as unknowns. Instead, constant values obtained from the satellite orbit geometry were used for these angles, and errors in these values will be absorbed by X_0 and Y_0 . As an alternative to this solution, the selection of estimable parameters and least squares solution could also be based on singular value decomposition and QR decomposition (CRESPI et al. 2008, p. 1324).

2.2 Mathematical Model using straight Lines

The line coplanarity model (LCM) is based on the coplanarity between the projection ray containing an image point (v_i) and the projection plane in the object space defined by an object line and the instantaneous PC.

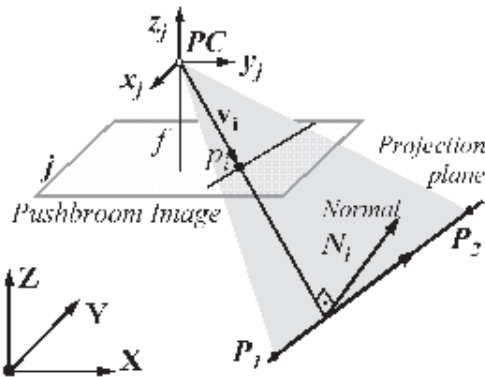


Fig. 1: The projection ray and the vector normal to the projection plane in the object space.

Based on this geometry, it follows that the vector normal to the projection plane in the object space must be orthogonal to the projection ray (Fig. 1).

The straight line in the object space is defined by P_1 and P_2 , and p_i is a point in the corresponding image line for a specific image row j (Fig. 1). There is no need for correspondence between points in the image with another one in the object space. This model was originally presented by MULAWA & MIKHAIL (1988) and HABIB et al. (2002).

The direction of projection ray (v_i) in object space is obtained by applying the rotation matrix R_j to the image point p_i . The orthogonality condition between v_i and the vector normal to the projection plane in object space (N_i) can be expressed by (4).

$$N_i \cdot R_j \begin{bmatrix} 0 \\ y_i \\ -f \end{bmatrix} = 0 \tag{4}$$

In (4), N_i is defined by the cross product of the direction vector $(P_2 - P_1)$ of the straight line and the vector difference between the instantaneous PC and point P_1 in the object straight line $(PC - P_1)$ (see Fig. 1); and $[0, y_i, -f]^T$ is the position vector of point p_i in the image space (projection ray).

A detailed description of this model is presented in TOMMASELLI & MEDEIROS (2010).

3 Experiments and Results

The models were implemented in the in-house developed software TMS (triangulation with multiple sensors), with multi-feature control (GCPs and GCLs). The parameters estimation method implemented in this software is the unified approach to least squares adjustment (MIKHAIL & ACKERMANN 1976, p.333). This method was used because several sources of data can be handled within the same software.

Experiments were conducted with a block composed of four level 1 (only with radiometric correction) CBERS-2B HRC images. These images were acquired in adjacent orbits (159 and 158). The images 159-E_125-1 (image 3) and 159-E_125-2 (image 1) were collected at the same day. However, images 158-A_125-1 (image 4) and 158-A_125-2 (image 2) were acquired on different dates. Fig. 2 shows the four images used in the experiments. Some technical specifications of HRC are presented in Tab. 1.

The control and check points were distinct points surveyed with a dual-frequency GPS, Hipper GGD. The GPS data were processed using the PPP (Precise Point Positioning) on-

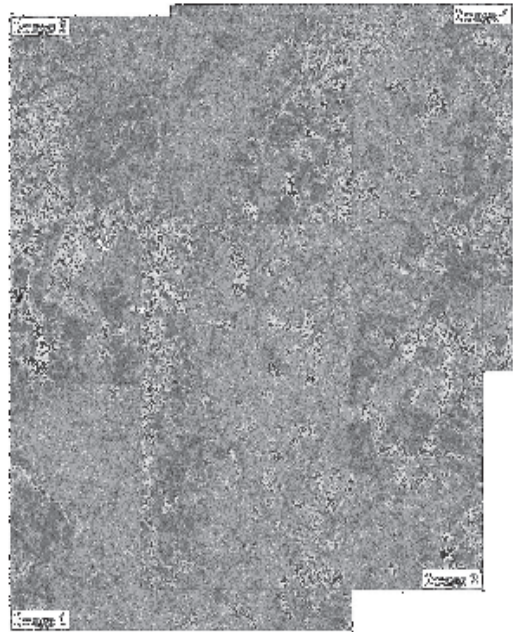


Fig. 2: Block composed by CBERS-2B HRC images used in the experiments.

Tab. 1: Technical features of CBERS-2B HRC (INPE, 2011).

Focal length (mm)	3398
Image level	1 (radiometric correction)
Image size (pixels)	12 246 × 12 246
GSD (m)	2.7
Orbital altitude (km)	778

line service available at the IBGE (Instituto Brasileiro de Geografia e Estatística – Brazilian Institute of Geography and Statistics) web site.

Object lines were defined by endpoints directly measured on road paths with GPS in kinematic mode. After processing the GPS data collected in kinematic mode, the resulting coordinates were filtered to remove points with a high standard deviation and to establish representative coordinates for each road straight line segment. In this last step, a 3D collinearity condition was applied among the road points to ensure that the points are on a straight line with a certain accuracy level. Fig. 3 depicts this condition. To verify whether or not point P_3 belongs to the straight line defined by points P_1 and P_2 , the orthogonal distance (L) of point (P_3) to the straight line and the vertical (θ) and horizontal (α) deflection angles were computed. Thus, by establishing proper thresholds ($T_L = \pm 2.5$ m; $T_\theta = \pm 0.2^\circ$; $T_\alpha = \pm 0.4^\circ$), it is possible to determine if the point actually belongs to the straight line.

After this analysis of road paths, the coordinates of the road centre were calculated by applying variable offsets, which were estimated through the average values of the distances

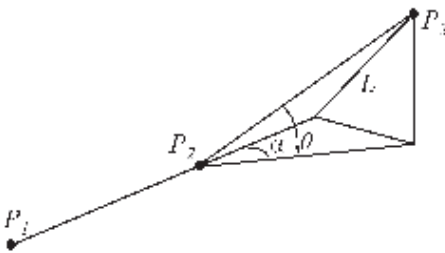


Fig. 3: Collinearity condition used to establish endpoints of control straight lines.

between the car paths along both directions on the road.

It is worth noting that a very dense cloud points can be surveyed on the ground, and from these points some suitable line segments are extracted automatically. The LCM, as presented in (4), requires only one image point belonging to that line segment. A second or a third point can be measured, providing more conditions equations, based on (4). From an operational point of view, it is quite straightforward to acquire GPS points while traveling from one control point to the next one. Additional paths can improve the number of control lines at a very reasonable cost-benefit ratio when comparing it to the measurement of a control point. Existing road base maps can also be used, provided that their quality is compatible to the images to be oriented.

Image coordinates of both GCPs and points belonging to an image line were measured interactively on-screen. It is important to note that well-defined lines and edges can be measured with subpixel precision using techniques of image processing, but in this case, the images have low contrast, making automation troublesome. For this reason, in all experiments presented in this paper, the on-screen measurement was conducted with at least two points per line.

Experiments using both models, collinearity (CMP) and coplanarity (LCM), for block adjustment were performed in addition to some experiments using different configurations of control entities. The main characteristics of these experiments are presented in Tab. 2. Finally, an experiment to assess the effects of relative misalignment of the CCD sensors in the CBERS-2B HRC focal plane was performed.

The first set of experiments was conducted with all available GCPs and GCLs (see Tab. 2) to serve as references. Fig. 4 shows the control points and lines configurations along the block used in the experiments.

For each experiment the position-rotation parameters (12 parameters, (3)) were estimated using both models ((1) and (4)) and datasets according to Tab. 2 and Fig. 4.

Ground coordinates of control points and endpoints of GCLs were introduced as relative constraints with standard deviations of 10 cm

Tab. 2: Number of GCPs and GCLs used in the experiments.

Experiment	A	B	C	D	E	F	G
	CMP	LCM					
Num. of GCPs	55	0	55	22	22	12	12
Num. of GCLs	0	73	73	0	73	0	73

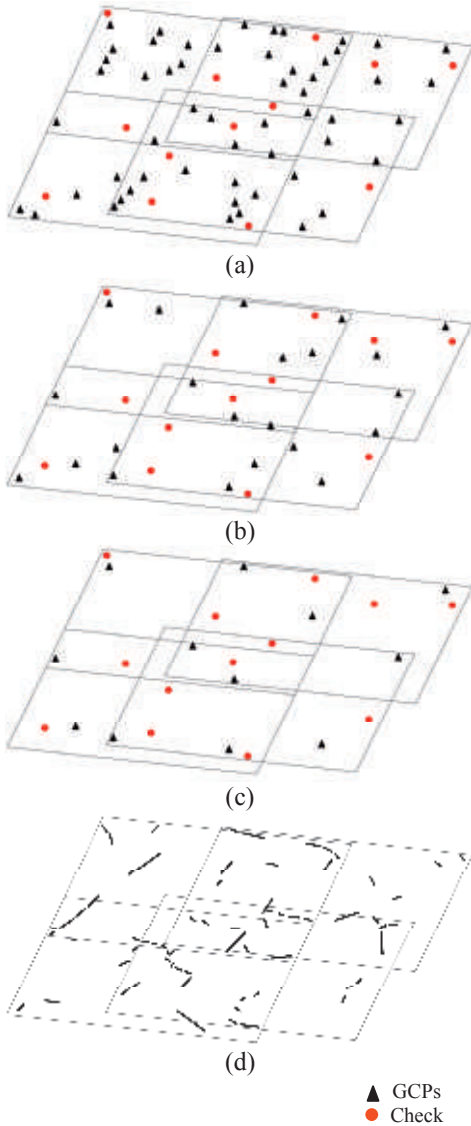


Fig. 4: Configurations of the control points, check points, and control lines used in the experiments: (a) 55 GCPs and 13 check points, (b) 22 GCPs and 13 check points, (c) 12 GCPs and 13 check points, (d) 73 GCLs.

in all components. This accuracy for the GCLs endpoints is optimistic considering the survey technique previously described. However, in the bundle adjustment the adjusted image coordinates and parameters will absorb the error in the GCLs coordinates. Geocentric Cartesian coordinates of all points (GCPs and endpoints of GCLs) were computed in the WGS84 reference frame. Thus, the parameters were also estimated in this reference frame.

The quality of the estimated parameters was assessed using 13 independent check points (Fig. 4a). The check points coordinates have the same accuracy as the GCPs because they were surveyed using the same technique.

First, both the coordinates of the check points and the estimated parameters were transformed to a local right-handed Cartesian System (Y axis in the direction of local north and Z axis aligned with the normal in the local origin). Then, the coordinates of these check points were computed by back-projecting image coordinates using the inverse form of the collinearity equations considering a known Z value in the local reference system. The discrepancies between the X and Y ground coordinates and those obtained with the inverse collinearity model were then computed.

Tab. 3 presents the RMSE (root-mean-square error) in the check point coordinates for each image of the reference experiments, in which all available GCPs and GCLs were used. In the last row of Tab. 3, we present the total RMSE, computed for all check points in the images. The results presented in Tab. 3 represent the final accuracy that would be achieved with such a procedure when using HRC images.

Tab. 3: RMSE (in GSD) in the check point coordinates (single-ray backprojection with a known elevation).

Image	A 55 GCPs		B 73 GCLs		C 55 GCPs 73 GCLs	
	X	Y	X	Y	X	Y
1	3.5	2.0	3.3	2.0	3.0	1.7
2	4.7	2.4	5.3	2.5	3.4	2.0
3	5.8	2.6	2.7	1.8	3.6	2.6
4	3.1	3.0	7.3	3.4	4.5	2.4
Total	4.1	2.4	4.7	2.3	3.4	2.1

The analysis of Tab. 3 shows that in some cases the CMP (GCPs) provided better results when compared to the LCM (GCLs). This finding was verified in image 4, in which the RMSE obtained with the CMP was 3.1 and 3.0 GSDs, while the RMSE for LCM was 7.3 and 3.4 in X and Y, respectively. In image 3, however, LCM provided better results compared to the CMP. These results are related to the geometric configurations of points and lines, as shown in Figs. 4 and 5, and for HRC images.

It was also verified that, in general, the combination of GCPs and GCLs reduced the RMSE in the check point coordinates.

Experiments reducing the number of GCPs were also accomplished (see Tab. 2 for the number of control entities and Fig. 4 to see the geometric configurations).

Tab. 4 presents the RMSE in the check point coordinates for the other experiments described in Tab. 2. Fig. 5 shows the resultant

Tab. 4: RMSE (in GSD) in the check points coordinates computed with parameters estimated in experiments D, E, F, and G.

	D		E		F		G	
	22 GCPs		22 GCPs 73 GCLs		12 GCPs		12 GCPs 73 GCLs	
Image	X	Y	X	Y	X	Y	X	Y
1	7.8	2.7	3.3	1.8	18.3	8.3	3.3	1.9
2	8.1	4.5	2.6	2.0	27.2	5.0	2.2	1.9
3	5.1	2.4	3.2	2.2	13.1	6.6	3.5	1.9
4	3.1	2.3	5.3	2.2	30.3	4.0	5.6	2.8
Total	5.9	2.9	3.5	1.9	21.7	5.8	3.6	2.0

Tab. 5: RMSE in the coordinates of the checkpoints computed with EOP estimated considering two sets of CCDs (central and lateral).

	Image 1		ncp	Image 2		ncp	Image 3		ncp	Image 4		ncp
	X	Y		X	Y		X	Y		X	Y	
Central CCD RMSE (GSD)	1.74	0.37	3	2.02	1.61	3	1.69	0.80	2	3.59	2.66	2
Lateral CCDS RMSE (GSD)	1.44	1.11	3	1.25	2.46	3	1.18	2.41	4	1.46	1.80	4
3 CCDS RMSE (GSD)	1.43	0.74		1.50	1.86		1.18	1.90		1.96	1.83	
Total (GSD)										1.4	1.5	

RMSE of the two coordinate components (X and Y) for all experiments.

As it was expected, Tab. 4 and Fig. 5 show that the RMSE in the check point coordinates increases as the number of GCPs decreases (experiments D and F). It was also verified that the combination of GCPs and GCLs improves the results. The results obtained by combin-

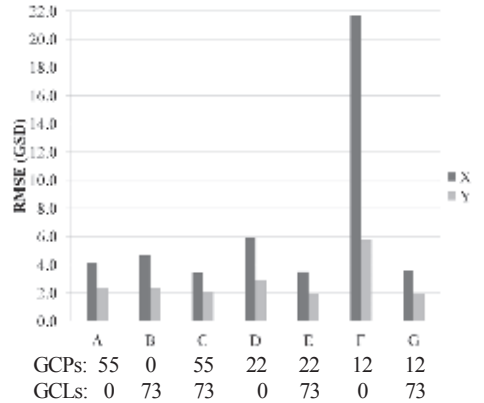


Fig. 5: RMSE in XY in check points for each experiment.

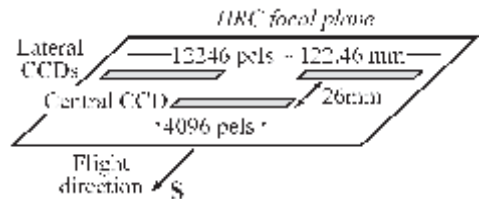


Fig. 6: HRC inner geometry, with the three CCDs in the focal plane.

ing 12 GCPs with 73 GCLs (experiment G) are approximately similar to those obtained with the total number of GCPs (experiment A – see Tab. 3 and Fig. 5).

The RMSE in the X coordinate for all experiments were larger than the RMSE in the Y coordinate. In general, the RMSE in X coordinate surpass 3 GSDs, indicating that a systematic error in the inner geometry of the HRC camera affected this coordinate.

As it was previously mentioned, the HRC sensor is composed of three matrices of CCD detectors. The two lateral matrices (1 and 3) are aligned, and the central matrix (2) is displaced by 26 mm along the flying direction (Fig. 6). The overlap between the images collected from each matrix is approximately 8.5 pixels. Techniques of area based matching and image transformation are applied to generate the virtual images with 12246 columns, which are made available to the users. An error in the inner geometry of the images is likely to occur, owing to the difference of approximately 0.89 seconds for the acquisition of the corresponding image rows of CCDs 1/3 and 2. As a consequence, the EOP are different for CCDs 1/3 and 2, and the image stitching procedure that is applied to match the three images cannot be sufficient to correct these differences.

To assess the quality of HRC imagery generation, experiments with two different datasets were accomplished: (1) all points and lines observations belonging only to the central CCD (columns 4082 to 8164) and (2) all points and lines observed in the lateral CCDs (columns: 0 to 4082 and 8164 to 12246).

The step previously described provides two sets of EOP, one for the lateral CCDs and another one for the central CCD.

The coordinates of the check points were then estimated through the back-ray projection procedure using both sets of EOP. Tab. 5 presents the RMSE in the 13 check point coordinates (X and Y in GSD) for each image and for check points lying in the coverage areas of the central CCD and lateral CCDs. The number of check points (ncp) is also presented in Tab. 5. In the central CCD of images 3 and 4, only 2 check points were available, but this small number did not affect significantly the results assessment. In Tab. 5, the total RMSE for all check points covered by the 3 CCDs,

though with their coordinates computed using two sets of EOP, are presented (Tab. 5, third row). Finally, the total RMSE, for all check points and all images was computed and are presented in the last row of Tab. 5.

Comparing the total RMSE of Tab. 5 with the RMSE of experiment C presented in Tab. 3, it can be observed that the former is 41 % of the value in X and 71 % of the value in Y.

The RMSE in check point coordinates showed that a better result is achieved when the images of the CCD matrices are processed in two separate runs. This result gives a strong indication that there is a systematic error caused by the image fusion.

In general, the RMSE in the check point coordinates are less than two GSDs (5 m). This result indicates that the generation of the virtual image introduces a systematic error in the inner geometry of the images, caused by the non-alignment of the CCDs of the sensor.

Finally, as it was previously mentioned, the CBERS-2B HRC camera presents a reduced dynamic range that affected the identification and measurement of control entities in the images. Although the nominal GSD of CBERS-2B HRC is 2.7 m, the EIFOV (effective instantaneous field of view) in the along- and across-track directions are approximately 4.1 m and 4.6 m, respectively. Therefore, it can be concluded that the results with GCPs and GCLs are near one EIFOV.

4 Conclusions

This paper presented an approach aimed at the indirect orientation of pushbroom images, using experiments performed with CBERS-2B HRC images. The mathematical models of collinearity and coplanarity for straight lines were used in an adapted form of triangulation of pushbroom images. Experiments using both the collinearity (CMP) and the coplanarity models (LCM) for a block composed of four CBERS-2B HRC images from two adjacent orbits were performed. The models were implemented using TMS software that uses multi-feature control (points and lines).

The results showed that the line coplanarity model works well in block adjustment with CBERS-2B HRC images.

The results showed that the combination of collinearity and line coplanarity models provided better results in the bundle block adjustment process than conventional bundle adjustment with GCPs only. A systematic error in the inner geometry of the HRC camera caused by the displacement of one of the three CCD sensors and the lack of proper correction when fusing the three images to generate level 1 virtual image was also verified.

The experiments show that the use of ground control lines could reduce or even eliminate the need for ground control points. The combination of both control entities is a good compromise, as it was shown in this study. In countries with deficient cartographic coverage, such as Brazil, techniques for fast image orientation are of great importance.

Techniques to improve and automate the measurement of image points and lines will be developed and the effects of introducing orbital data in the bundle adjustment will be assessed in future work. It is important to mention that the CBERS-2B HRC was an experimental camera that was not developed for commercial purposes.

Acknowledgements

The authors would like to acknowledge the support of FAPESP (Fundação de Amparo à Pesquisa do Estado de São Paulo) through a Master Scholarship, and CNPq (Conselho Nacional de Desenvolvimento Científico e Tecnológico) through Research Grants.

References

- BALTSAVIAS, E., LI, Z. & EISENBEISS, H., 2006: DSM Generation and Interior Orientation Determination of IKONOS Images Using a Testfield in Switzerland. – *PFG* **1/2006**: 41–54.
- CRESPI, M., FRATARCANGELI, F., GIANNONE, F., COLOSIMO, G., PIERALICE, F. & JACOBSEN, K., 2008: Geometric potential of Cartosat-1 stereo imagery. – *International Archives of Photogrammetry and Remote Sensing* **37** (B1): 1323–1330.
- DOWMAN, I. & MICHALIS, P., 2003: Generic rigorous model for along track stereo satellite sensors. – *ISPRS Workshop on High Resolution Mapping from Space*, Hannover, Germany.
- FRASER, C.S. & HANLEY, H.B., 2005: Bias-compensated RPCs for Sensor Orientation of High-resolution Satellite Imagery. – *Photogrammetric Engineering and Remote Sensing* **71** (8): 909–915.
- FRITSCH, D. & STALLMANN, D., 2000: Rigorous photogrammetric processing of high resolution satellite imagery. – *International Archives of Photogrammetry and Remote Sensing* **33** (B1): 313–321.
- GUGAN, D.J. & DOWMAN, I.J., 1988: Accuracy and completeness of topographic mapping from SPOT imagery. – *Photogrammetric Record* **12** (72): 787–796.
- HABIB, A., LEE, Y. & MORGAN, M., 2001: Bundle Adjustment with Self-Calibration of Line Cameras using Straight Lines. – *Joint Workshop of ISPRS WG 1/2, 1/5 and 1/7: High Resolution Mapping from Space*, University of Hannover.
- HABIB, A., MORGAN, M. & LEE, Y., 2002: Bundle Adjustment with Self-Calibration using Straight Lines. – *Photogrammetric Record* **17** (100): 635–650.
- HABIB, A. & MORGAN, M.F., 2003: Linear Features in Photogrammetry. – *Boletim de Ciências Geodésicas* **9** (1): 3–24.
- INPE, 2011: CBERS – China-Brazil Earth Resources Satellite. – <http://www.cbers.inpe.br>. (10.11.2011).
- KIM, T. & DOWMAN, I., 2006: Comparison of two physical sensor models for satellite images: Position-Rotation model and Orbit-Attitude model. – *The Photogrammetric Record* **21** (114): 110–123.
- LIU, S., FRASER, C.S., ZHANG, C. & RAVANBAKHS, M., 2011: Georeferencing performance of Theos Satellite Imagery. – *The Photogrammetric Record* **26** (134): 250–262.
- MARCATO JUNIOR, J., TOMMASSELLI, A.M.G., MEDEIROS, N.G. & OLIVEIRA, R.A., 2010: Bundle Block Adjustment of CBERS 2B HRC Images using Control Lines. – *The International Archives of Photogrammetry and Remote Sensing*, Calgary **XXXVIII** (1), unpaginated CD.
- MIKHAIL, E.M. & ACKERMANN, F., 1976: *Observations and Least Squares*. – 1st ed., 497 p., IEP, New York.
- MULAWA, D.C. & MIKHAIL, E.M., 1988: Photogrammetric treatment of linear features. – *The International Archives of Photogrammetry and Remote Sensing* **III**: 383–393, Kyoto.
- ORUN, A.B. & NATARAJAN, K., 1994: A modified bundle adjustment software for SPOT imagery and photography: tradeoff. – *Photogrammetric*

- Engineering & Remote Sensing **60** (12): 1431–1437.
- POLI, D., 2007: A Rigorous Model for Spaceborne Linear Array Sensors. – *Photogrammetric Engineering & Remote Sensing* **73** (2): 187–196.
- RADHADEVI, P.V., SASIKUMAR, T.P. & RAMACHANDRAN, R., 1994: Orbit attitude modelling and derivation of ground co-ordinates from spot stereopairs. – *ISPRS Journal of Photogrammetry and Remote Sensing* **49** (4): 22–28.
- ROTTENSTEINER, F., WESER, T., LEWIS, A. & FRASER, C.S., 2009: A Strip Adjustment Approach for Precise Georeferencing of ALOS Optical Imagery. – *IEEE Transactions on Geoscience and Remote Sensing* **47** (12): 4083–4091.
- SHIN, S.W., HABIB, A.F., GHANMA, M., KIM, G. & KIM, E.M., 2007: Algorithms for Multi-sensor and Multi-primitive Photogrammetric Triangulation. – *ETRI Journal* **29** (4): 411–420.
- TOMMASELLI, A.M.G. & TOZZI, C.L., 1996: A recursive approach to space resection using straight lines. – *Photogrammetric Engineering & Remote Sensing* **62** (1): 57–66.
- TOMMASELLI, A.M.G. & MEDEIROS, N.G., 2010: Determination of the indirect orientation of orbital pushbroom images using control straight lines. – *Photogrammetric Record* **25** (130): 159–179.
- TONG, X., LIU, S. & WENG, Q., 2010: Bias-corrected rational polynomial coefficients for high accuracy geo-positioning of QuickBird stereo imagery. – *ISPRS Journal of Photogrammetry and Remote Sensing* **65** (2): 218–226.
- TOUTIN, T. & ROCHON G., 1986: SPOT a new cartographic toll. – *The International Archives of Photogrammetry and Remote Sensing*, Edinburgh, Scotland **26** (4): 192–205.
- TOUTIN, T., 2003: Block Bundle Adjustment of Landsat 7 ETM+ Images over Mountainous Areas. – *Photogrammetric Engineering & Remote Sensing* **69** (12): 1341–1349.
- TOUTIN, T., 2004: Geometric processing of remote sensing images: models, algorithms and methods. – *International Journal of Remote Sensing* **25** (10): 1893–1924.
- TOUTIN, T., 2006: Comparison of 3D Physical and Empirical Models for Generating DSMs from Stereo HR images. – *Photogrammetric Engineering and Remote Sensing* **72** (5): 597–604.
- WESER, T., ROTTENSTEINER, F., WILLNEFF, J., POON, J. & FRASER, C.S., 2008: Development and testing of a generic sensor model for pushbroom satellite imagery. – *The Photogrammetric Record* **23** (123): 255–274.
- YU, J., YUAN, X. & ZHENLI, W., 2008: Calibration of constant angular error for CBERS-2 imagery with few ground control points. – *The International Archives of Photogrammetry and Remote Sensing* **37** (B1): 769–774, Beijing.

Address of the authors:

Prof. Dr. ANTONIO M. G. TOMMASELLI, tomaseli@fct.unesp.br, Eng. Ms. JOSÉ MARCATO JUNIOR, jrmarcato@gmail.com, Dept. of Cartography, UNESP – Universidade Estadual Paulista, Rua Roberto Simonsen 305, Presidente Prudente, São Paulo, Brasilien

Manuskript eingereicht: November 2011
Angenommen: Januar 2012